www.czasopisma.pan.pl PAN POLSKA AKADEMIA NAUK www.journals.pan.pl

Arch. Metall. Mater. **65** (2020), 3, 1023-1028

DOI: 10.24425/amm.2020.133211

SUN-WOO BAE[1], XUAN-KHOA HUYNH[2], JI-SOON KIM[1*]

EFFECT OF FABRICATION METHOD OF Fe-TiB_2 NANOCOMPOSITE POWDERS ON SPARK-PLASMA SINTERING BEHAVIOR

In this study, Fe-40wt% TiB_2 nanocomposite powders were fabricated by two different methods: (1) conventional powder metallurgical process by simple high-energy ball-milling of Fe and TiB_2 elemental powders (*ex-situ* method) and (2) high-energy ball-milling of the powder mixture of (FeB+TiH_2) followed by reaction synthesis at high temperature (*in-situ* method). The *ex-situ* powder was prepared by planetary ball-milling at 700 rpm for 2 h under an Ar-gas atmosphere. The *in-situ* powder was prepared under the same milling condition and heat-treated at 900°C for 2 h under flowing argon gas in a tube furnace to form TiB_2 particulates through a reaction between FeB and Ti. Both Fe-TiB_2 composite powder compacts were sintered by a spark-plasma sintering (SPS) process. Sintering was performed at 1150°C for the *ex-situ* powder compact and at 1080°C for the *in-situ* powder for 10 minutes under 50 MPa of sintering pressure and 0.1 Pa vacuum for both processes. The heating rate was 50°/min to reach the sintering temperature. Results from analysis of shrinkage and microstructural observation showed that the *in-situ* composite powder compacts had a homogeneous and fine microstructure compared to the *ex-situ* preparation, even though the sintered densities were almost the same (99.6 and 99.8% relative density, respectively).

Keywords: Fe-TiB_2 composite, *ex-situ*, *in-situ*, iron boride, titanium hydride, high-energy ball-milling, spark-plasma sintering, densification behavior

1. Introduction

The Fe-TiB_2 composite materials tend to have many good mechanical properties such as high hardness, strength, toughness, relatively good thermal stability, and low cost materials. Various fabrication methods have been reported, including laser cladding [1-2], plasma transferred arc (PTA) [3-4], aluminothermic reduction [5], spark plasma sintering (SPS) [6], and self-propagating high-temperature synthesis (SHS) [7-10]. The most important prerequisite for structural composite materials is a microstructure composed of ductile matrix reinforced with a homogeneous distribution of ultrafine hard particulates. In this sense, the *in-situ* technique has many advantages for fabricating composite materials, such as reduction of reinforcement size with a narrow size distribution, even dispersion of reinforcements, and a clean interface between the reinforcement-matrix with high interfacial strength [11].

We have also reported that Fe-TiB_2 composite powder with TiB_2 particulates smaller than 5 nm could be synthesized *in-situ* by planetary ball milling and subsequent heat treatment of an iron boride (FeB) and titanium hydride (TiH_2) powder mixture [12]. The effect of mechanical activation on the *in-situ* formation of TiB_2 particulates in the powder mixture of TiH_2 and FeB has been reported, and the interface reactions between Ti and FeB powders were explained in detail [13].

Our previous works on the sintering of (FeB + TiH_2) powder mixtures by pressureless sintering and spark-plasma sintering showed that nanoscale Fe-TiB_2 composite materials can be fabricated through a relatively simple powder metallurgy process. Thus, it was expected that enhancement of densification can occur through the self-propagating high-temperature synthesis reaction to form TiB_2 phase in Fe-matrix by the reaction between FeB and TiH_2 during the sintering process [14-15]. In the case of pressureless sintering, we obtained a maximum sintered density of 96% relative density (RD) at a high sintering temperature of 1400°C for a long sintering time of 2 hours. The size of TiB_2 particulates in the Fe-matrix had grown to several micrometers after sintering [14]. The effectiveness of spark plasma sintering for the same (FeB + TiH_2) powder mixtures was evident. A higher sintered density of 98% RD was obtained after sintering

[1] UNIVERSITY OF ULSAN, SCHOOL OF MATERIALS SCIENCE AND ENGINEERING, 55 BON-GIL 12, TECHNOSANEOP-RO, NAM-GU, ULSAN 44776, KOREA
[2] INDUSTRIAL UNIVERSITY OF HO CHI MINH CITY, FACULTY OF MECHANICAL TECHNOLOGY, HO CHI MINH CITY, VIETNAM

* Corresponding author: jskim@ulsan.ac.kr

© 2020. The Author(s). This is an open-access article distributed under the terms of the Creative Commons Attribution-NonCommercial License (CC BY-NC 4.0, https://creativecommons.org/licenses/by-nc/4.0/deed.en which permits the use, redistribution of the material in any medium or format, transforming and building upon the material, provided that the article is properly cited, the use is noncommercial, and no modifications or adaptations are made.

at a lower temperature of 1150°C for 15 min. The microstructural observation of sintered compacts with use of FE-SEM and HR-TEM revealed that ultrafine particulates of approximately 5 nm diameter were evenly distributed in an Fe-matrix [15]. Such a microstructure gives rise to excellent mechanical and tribological properties [16]. It should be noted here that all the sintering studies mentioned above were performed for (FeB + TiH_2) powder mixtures without any pre-reaction to form TiB_2.

The aim of this work is to study the spark-plasma sintering behavior of *in-situ* synthesized Fe-TiB_2 composite powder and ex-situ processed composite powder. To demonstrate the effectiveness of the *in-situ* process on the sintering behavior compared to the *ex-situ* process, shrinkage, densification rate, sintered density, and microstructure are investigated.

2. Experimental procedure

The Fe-40wt% TiB_2 nanocomposite powders were fabricated by *ex-situ* and *in-situ* methods. The (a) *ex-situ* method is a conventional powder metallurgical process using simple high-energy ball-milling of Fe and TiB_2 elemental powders, while (b) the *in-situ* method involves high-energy ball-milling of the powder mixture of (FeB+TiH_2) followed by a reaction synthesis at high temperature.

The *ex-situ* powder was prepared by planetary ball-milling at 700 rpm for 2 h under an Ar-gas atmosphere. The *in-situ* powder was prepared under the same milling condition and then heat-treated at 900°C for 2 h under flowing argon gas in a tube furnace to form TiB_2 particulates through a reaction between FeB and Ti. More details of the fabrication process of the (FeB, TiH_2) powder mixture can be found in our previous works [12,13].

Both Fe-TiB_2 composite powder compacts were sintered by a spark-plasma sintering (SPS) process. The powders were loaded into cylindrical graphite dies and heated at a rate of 50°C/min. Sintering was performed at 1150°C for the *ex-situ* powder and at 1080°C for the *in-situ* powder. Different sintering temperatures were chosen to obtain full density. A constant pressure of 50 MPa in a vacuum chamber of 0.1 Pa was applied for all sintering experiments. The data on shrinkage displacement, temperature, vacuum condition, pulse voltage, and current were digitally stored by a data acquisition system and used for further analysis. The change in shrinkage displacement and its derivative (densification rate) as a function of temperature and time were obtained. The fracture surfaces of some selected sintered compacts and the polished cross-sections of the fully densified compacts were observed by FE-SEM.

3. Results and discussion

Figure 1 shows the changes in shrinkage displacement and its derivative (densification rate) of the *ex-situ* processed Fe-40wt% TiB_2 powder compact during the spark-plasma sintering process. The shrinkage displacement curve showed two rapid densification events at 500-800°C and 900-1070°C. These two fast densification events were confirmed in the densification rate curve. The densification quickly proceeded and resulted in a sintered density of 90.6% at 1070°C. Further heating to 1150°C with a holding time of 10 minutes led to an increase in sintered density up to 99.6%.

To thoroughly investigate the sintering behavior, the fracture surfaces of some selected sintered compacts were observed by FE-SEM. The results are shown in Fig. 2. As discussed above, the first shrinkage was observed between 500-800°C. The specimen sintered at 830°C (Fig. 2(a)) showed a sintered density of 68.2% and typical microstructure of a green metal powder compact. Agglomerated powders contacted only one another. No neck formation was observed between powders. Most of the shrinkage seemed to result from rearrangement of powder particles enhanced by the applied sintering pressure. Increasing the temperature could also enhance the shrinkage by increasing ductility of Fe-TiB_2 composite powders.

The second fast shrinkage between 900-1070°C could be explained by the normal densification process and neck formation and growth between the powders. Even though the microstructure of the specimen sintered at 973°C (Fig. 2(b)) was composed of mostly pores, partial neck areas were formed between powder agglomerates, which led to easy fracture. The further increase of sintering temperature to 1070°C (Fig. 2(c)) enhanced the den-

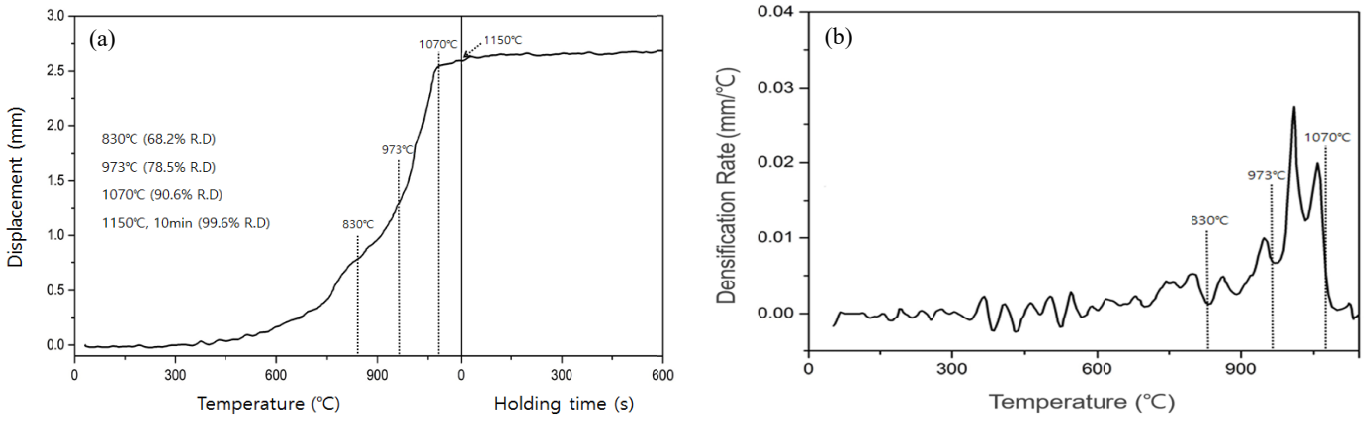

Fig. 1. Changes of shrinkage displacement and its derivative (densification rate) during spark-plasma sintering of the *ex-situ* powder compact. The Fe and TiB_2 elemental powder compact was heated to 1150°C at a rate of 50°C /min under a sintering pressure of 50 MPa and then held for 10 min

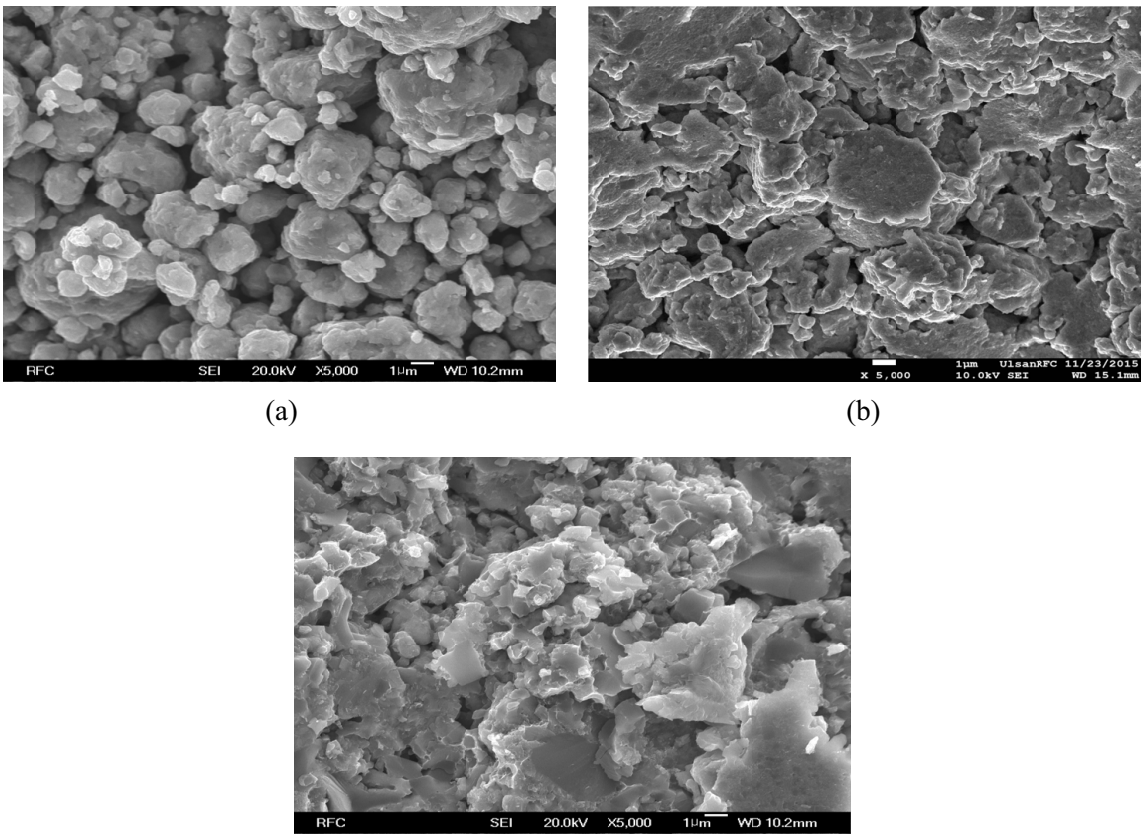

(a) (b)

(c)

Fig. 2. FE-SEM secondary-electron images of the fractured surfaces of the *ex-situ* powder compacts spark-plasma sintered at various temperatures for 0 min. (a) 830°C (68.2% relative density, RD), (b) 973°C (78.5% RD), and (c) 1070°C (90.6% RD)

sification process. The sintered density increased drastically to 90.6% RD, and the microstructure changed to a larger neck area. A full density of 99.6% was obtained at 1150°C for 10 minutes.

Figure 3 shows a secondary electron image and a back-scattered electron image of the polished cross-section of the *ex-situ* processed powder compact sintered at 1150°C for 10 minutes with 99.6% relative density. We observed three phases with different gray levels, as reported in our previous works [12,13]: dark gray, gray, and bright gray. The dark-gray phase was TiB_2 containing the B element with a small atomic number of 5, while the bright-gray phase was relatively large Fe-powders with the atomic number of 26. It seemed that the TiB_2 powders could not be completely destroyed even after intense high-energy ball-milling, and the large Fe powders also remained. The gray matrix areas were composed of finely dispersed Fe and TiB_2 particulates.

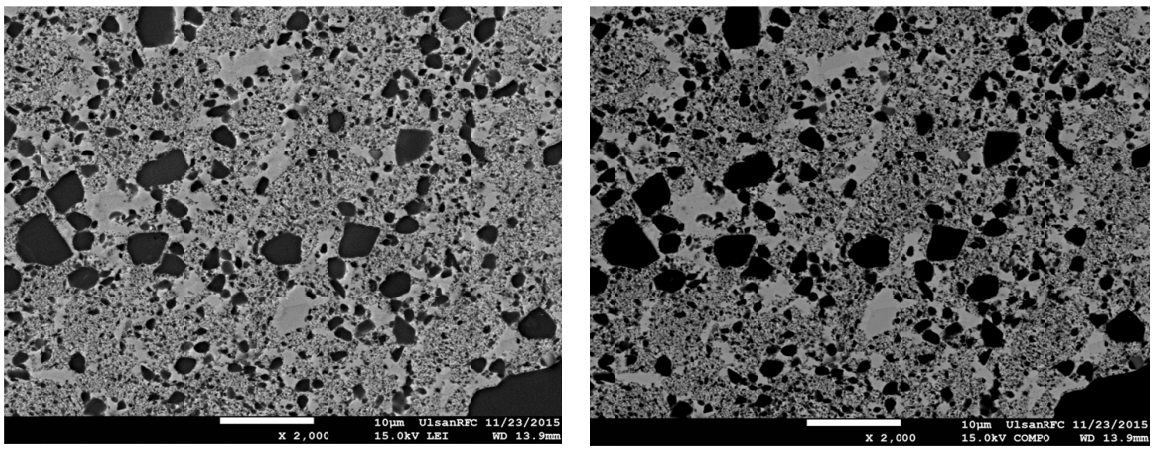

(a) (b)

Fig. 3. FE-SEM images of the polished cross-section of *ex-situ* powder compacts sintered at 1150°C for 10 min: (a) secondary electron image and (b) back-scattered electron image

Figure 4 shows the changes in shrinkage displacement and its derivative (densification rate) of the *in-situ* processed Fe-TiB_2 powder during the spark-plasma sintering process. Shrinkage started approximately at 700°C and showed only one maximum near 1000°C. Densification proceeded very quickly and resulted in a sintered density of 93.9% at 1080°C. Further holding at the same temperature for 10 minutes led to an increase in sintered density to 99.8%. This result is very different from the sintering behavior of the ex-situ powder and those reported in our previous works on the (FeB + TiH_2) powder mixture, where a lower sintered density of 98% RD was obtained at a higher sintering temperature of 1150°C [15]. It can be concluded that the self-propagating high-temperature synthesis reaction during spark-plasma sintering would have less effect on the sinterability of the (FeB+TiH_2) powder mixture than expected.

To further investigate the sintering behavior, the fracture surfaces of some selected sintered compacts of *in-situ* processed powders were observed by FE-SEM (Fig. 5). As shown in Fig 5(a), the shape and size of the composite powders are different from those of the *ex-situ* powders (Fig. 2(a)). While the

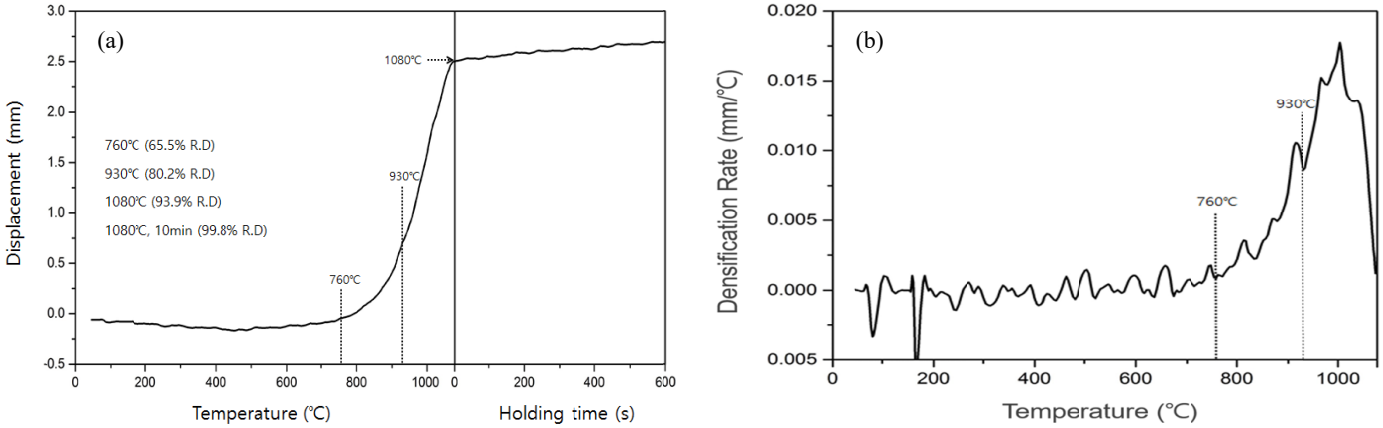

Fig. 4. Changes of shrinkage displacement and its derivative (densification rate) during spark-plasma sintering of the *in-situ* powder compact. The TiB_2 in Fe powder compact was heated to 1080°C at a rate of 50°C /min under a sintering pressure of 50 MPa and then held for 10 min

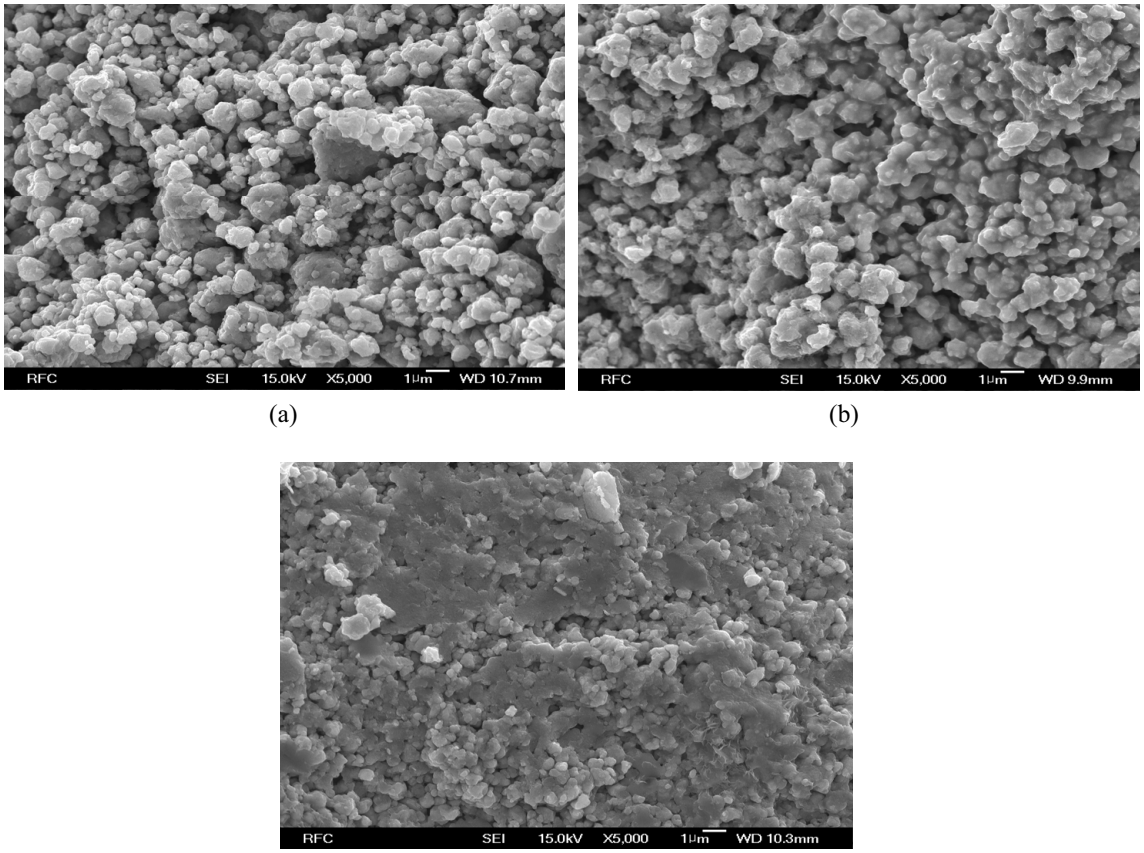

Fig. 5. FE-SEM secondary-electron images of the fractured surfaces of *in-situ* powder compacts spark-plasma sintered at various temperature for 0 min. (a) 760°C (65.5% relative density, RD), (b) 930°C (80.3% RD), and (c) 1080°C (93.9% RD)

ex-situ powders were agglomerated with a particle size of several micrometers, the *in-situ* powders were composed of many small particulates with more homogeneous size distribution. These effects led to the different sintering behaviors. Rearrangement of powders could be enhanced by the non-uniform size distribution of *ex-situ* powder and thereby to dense packing and greater shrinkage. Additionally, discretely existing large TiB_2 particulates in the *ex-situ* Fe-TiB_2 powder were more easily deformed by the external sintering pressure. On the contrary, the *in-situ* powder of very fine and uniform TiB_2 particulates in the Fe matrix should reveal a relatively lower green density and difficulty in rearrangement and deformation of powders, leading to a low densification, especially at the early stage of sintering. However, these effects could positively modify the densification at the middle and final stages of sintering, as observed in Fig. 5(b) and (c). The microstructure of the specimen sintered at 930°C (Fig. 5(b)) showed uniformly formed necks between the powders (80.2% RD). The specimen sintered at 1080°C (Fig. 5(c)) showed wide dense regions with small pores (93.9% RD). A full density of 99.8% RD was obtained after sintering at 1080°C for 10 minutes.

Figure 6 shows a secondary electron image and a back-scattered electron image of the polished cross-section of *in-situ* processed powder compact sintered at 1080°C for 10 minutes with 99.8% relative density. It shows a very different microstructure from the *ex-situ* processed sample (Fig. 3). No large particulates of TiB_2 were observed. We observed a very fine microstructure consisting of only two areas with different gray levels of gray and bright gray. Most areas were composed of the gray phase, which contains Fe and TiB_2. The bright-gray area is comprised of Fe-rich particles [13].

Figure 7 shows high-resolution TEM images of *in-situ* processed powder compact sintered at 1080°C for 10 minutes with 99.8% relative density. Microstructure is almost the same as the one reported in our previous work on the spark-plasma sintering of (FeB + TiH_2) powder mixture [15]. Dark particulates

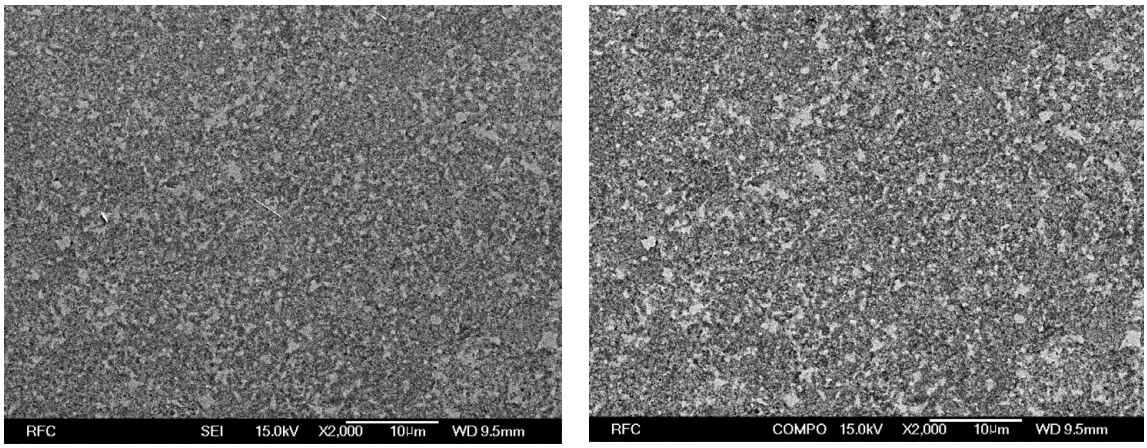

(a) (b)

Fig. 6. FE-SEM images of the polished cross-section of the *in-situ* powder compacts sintered at 1080°C for 10 min: (a) secondary electron image and (b) back-scattered electron image

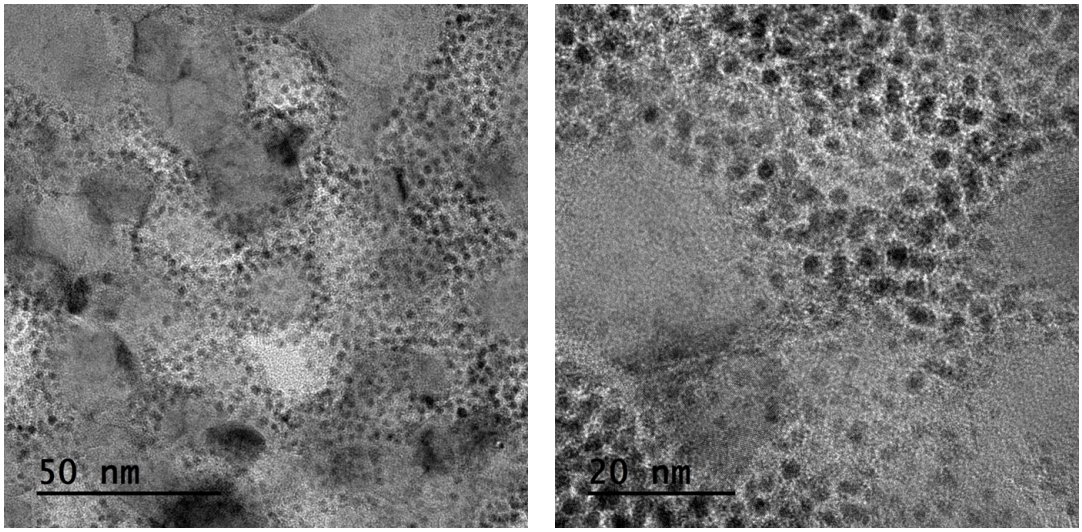

(a) (b)

Fig. 7. HR-TEM images of the *in-situ* powder compacts sintered at 1080°C for 10 min: (a) ×150,000 and (b) ×300,000

of TiB_2 with approximately 5 nm diameter are homogeneously distributed in the Fe-matrix. The more detailed explanation for analysis method has also been given in that previous work.

4. Conclusions

The effect of fabrication method for Fe-40wt% TiB_2 nanocomposite powders on spark-plasma sintering behavior was studied. From the results, the following conclusions were drawn.

(1) The effectiveness of spark-plasma sintering was evident. A full density of 99.6 and 99.8% RD was obtained for the *ex-situ* and the *in-situ* processed Fe-TiB_2 composite powders, respectively. In the in-situ sample, the microstructure showed an even distribution of very fine TiB_2 particulates with approximately 5 nm diameter.

(2) The *ex-situ* and the *in-situ* processed Fe-TiB_2 composite powders showed a difference in spark-plasma sintering behavior. Notably, the early stage of sintering for the *ex-situ* powder showed shrinkage by arrangement and deformation of agglomerated particles. Even though the in-situ powder did not show such effects, the fine size and uniform distribution of TiB_2 particulates enhanced the densification for a full-density and fine microstructure.

Acknowledgements

This work was supported by the 2018 Research Fund of University of Ulsan.

REFERENCES

[1] B. Du, Z. Zou, X. Wang, S. Qu, Appl. Surf. Sci. **254**, 6489-6494 (2008).
[2] B. Du, Z. Zou, X. Wang, S. Qu, Mat. Lett. **62**, 689-691 (2008).
[3] M. Darabara, G.D. Papadimitriou, L. Bourithis, Surf. Coat. Technol. **201**, 3518-3523 (2006).
[4] W. Xibao, W. Xiaofeng, S. Zhongquan, Surf. Coat. Technol. **192**, 257-262 (2005).
[5] A. Anal, T.K. Bandyopadhyay, K. Das, J. Mater. Process. Technol. **172**, 70-76 (2006).
[6] B. Li, Y. Liu, H. Cao, L. He, J. Li, J. Mater. Sci. **44**, 3909-3912 (2009).
[7] O.K. Lepakova, L.G. Raskolenko, Y.M. Maksimov, Combust., Explos. Shock Waves **36**, 575-581 (2000).
[8] C.C. Degnan, P.H. Shipway, Metall. Mater. Trans. A **33**, 2973-2983 (2002).
[9] L. Gai, M. Ziemnicka-Sylwester, Int. J. Refract. Met. Hard Mater. **45**, 141-146 (2014).
[10] O.K. Lepakova, L.G. Raskolenko, Y.M. Maksimov, J. Mater. Sci. **39**, 3723-3732 (2004).
[11] R.M. Aikin, JOM **49**, 35-39 (1997).
[12] X.K. Huynh, S.W. Bae, J.S. Kim, Korean J. Met. Mater. **55**, 10-15 (2017).
[13] X.K. Huynh, S.W. Bae, J.S. Kim, Arch. Metall. Mater. **62**, 1393-1398 (2017).
[14] X.K. Huynh, J.S. Kim, J. Korean Powder Metall. Inst. **23**, 282-286 (2016).
[15] X.K. Huynh, B.W. Kim, J.S. Kim, Arch. Metall. Mater. **63**, 1043-1047 (2018).
[16] H.R. Cho, J.S. Kim, K.H. Chung, Tribology International **131**, 83-93 (2019).